Available online at www.sciencedirect.com
SCIENCE DIRECT®
Catalysis Today 91–92 (2004) 59–65
CATALYSIS TODAY
www.elsevier.com/locate/cattod

Structured catalyst carrier for selective oxidation of hydrocarbons: modelling and testing

Andrzej Kołodziej [a], Waldemar Krajewski [a], Joanna Łojewska [b,*]

[a] *Institute of Chemical Engineering PAS, ul. Bałtycka 5, Pl 44-100 Gliwice, Poland*
[b] *Faculty of Chemistry, Jagiellonian University, Ingardena 3, 30060 Cracow, Poland*

Abstract

Metallic structured reactors have proved to increase the yield of maleic anhydride (MA) in oxidation of *n*-butane and to reduce catalyst deactivation. In this study a structured reactor made of Cr–Al steel rosettes has been tested. Reaction conditions (temperature, contact time, content of reaction mixture) were found to achieve optimal reactor performance. Based on obtained results a model of heat and mass transfer in the reactor has been put forward. The estimated activation energy of the *n*-butane oxidation to MA, 87 kJ/mol, agrees with the literature data.

Keywords: Catalytic oxidation; Heterogeneous catalysis; Maleic anhydride; Kinetic; Wash-coat depositing; V–P–O catalyst

1. Introduction

In recent years, more attention has been given to selective catalytic oxidation of hydrocarbons. One of the industrial challenges, maleic anhydride (MA), is obtained in catalytic oxidation of benzene or *n*-butane with oxygen from air [1]. On industrial scale, the process is carried out in multitubular reactors filled with tubes of 21 or 23.9 mm in i.d. [2]. The reactor operates at a temperature maintained precisely in the range of 350–370 °C, which is controlled by the circulation of molten salts in a cooling bath. A great deal of attention has also been given to developing the catalysts of high activity and selectivity towards MA. Typically used catalysts contain vanadium–phosphorus–oxide (V–P–O) doped with Fe, Cr, Ti, Co, Ni, Mo [3]; the active sites being assigned to vanadyl pyrophosphate $(VO)_2P_2O_7$ with vanadium at +4 oxidation state [4].

Although the process of *n*-butane oxidation to MA is mainly performed using bulk V–P–O catalyst (extruded in shapes of cylinders, spheres or rings) in multitubular fixed-bed reactors, there are great many examples of similar industrial large-scale processes which apply supported vanadium catalyst, e.g. *o*-xylene oxidation to phthalic anhydride or ethylene oxide production. For the *o*-xylene process the used Ti–V oxide catalyst is mainly deposited on small ceramic particles. Supported V–P–O catalysts are commonly applied for benzene oxidation to MA. There are also limited information about V–P–O catalyst deposited on ceramic particles [5] and alumina-, silica- and titania-supported V–P–O catalysts [6] used for *n*-butane to MA oxidation.

Metal structured carriers appear an attractive alternative for selective oxidation processes. The main problem encountered for selective oxidation is a low selectivity towards oxygenates resulting mainly from the kinetic control and temperature profile along the reactor. Additionally, in the industrial multitubular reactor with a ceramic carrier, hot-spots occur, which give rise to the deactivation of a catalyst due to the insufficient heat transfer, leading in turn to almost total oxidation of feed hydrocarbons, and in this way to a considerable decrease in yield. Thus, the selectivity can be increased by either choosing appropriate reaction conditions or by designing a proper structured reactor. There are, however, certain restrictions, which have to be taken into account to achieve this. High flow rates of reactants impose the selection of the catalyst carriers of an extra low pressure drop and high heat transfer coefficients from bed to cooling medium. Recently introduced chromium–aluminium steel leaves seem promising both for modelling optimal catalyst carriers and for catalyst deposition.

* Corresponding author. Tel.: +48-12-6324888; fax: +48-12-6340515.
E-mail address: lojewska@chemia.uj.edu.pl (J. Łojewska).

0920-5861/$ – see front matter © 2004 Elsevier B.V. All rights reserved.
doi:10.1016/j.cattod.2004.03.010

Nomenclature

a	specific catalyst surface (m^2/m^3)
C	concentration ($kmol/m^3$)
C_{Ac}	concentration of component A on catalytic surface ($kmol/m^3$)
D	reactor's diameter (m)
E	activation energy (kJ/mol)
k_{cv}	volumetric mass transfer coefficient to catalyst surface, (s^{-1})
k_1, k_2	kinetic rate constants of reaction (1a) and (1b) (s^{-1})
k_∞	pre-exponential coefficient in Arrhenius equation (s^{-1})
k_1^D	corrected kinetic rate constant, Eq. (4), (s^{-1})
L	reactor's length (m)
Q_R, Q_S	heat of reaction (1a) to MA, and (1b) to CO_2, respectively (kJ/mol)
r	kinetic rate kmol/(s m^3 of reactor)
T_f, T_c, T_w	temperatures of flowing gas, catalyst surface, reactor's wall, respectively (K)
w	superficial gas velocity (m/s)
x	axial coordinate (m)
X_D	diffusional correction factor (dimensionless)

Greek letters

α_c, α_w	heat transfer coefficient to catalyst surface, reactor's wall, respectively ($Wm^{-2}\,K^{-1}$)
ϵ	void volume (dimensionless)
η	conversion degree (dimensionless)
ν	stoichiometric coefficient in Eq. (1) (dimensionless)
τ	time (s)

Subscripts

A	*n*-butane
c	catalyst surface
f	flowing gas
R	MA
S	CO_2
w	tube's wall
0	inlet of reactor
1, 2	reactions (1a) and (1b), respectively

This paper poses a continuation of our project on the development of structured catalyst carriers for catalytic oxidation of hydrocarbons. The main aim of our project was to prove the applicability of metal structured catalyst for selective oxidation process. There we focused on three points: to deposit an oxide catalyst (typical of selective oxidation processes) on the metal surface; to test the catalyst deposited on metal structured carrier in selective oxidation (e.g. *n*-butane to maleic anhydride); to show the way of possibilities of enhancement of the heat and flow properties of the reactor by use of the structured catalyst. The aim of this study is to develop and to test the model of heat and mass transfer throughout the reactor using an approximation of parallel reaction kinetics and of uni-dimensional reactor. In this study, *n*-butane oxidation to MA over V–P–O catalyst has been chosen as a model process to test the carrier designed by us and to prove applicability of such a device to selective oxidation. For reference, we utilised some experimental results performed within another project using the same chemical reaction, equipment and V–P–O catalyst deposited on ceramic particles (unpublished data, which could be cited here only qualitatively).

2. Heat and flow characteristics of the designed carrier

Out of a great many structured carriers manufactured from Cr–Al steel leaves (steel type 00H20J5) studied so far [7], we have chosen the optimal one for this test reaction (7B). The best carrier has been chosen using performance efficiency criteria described in [8,9].

The carrier is built of rosettes and U-shaped rings. A rosette contains 20 leaves 9.2 mm in height and has a total diameter 23.9 mm (i.d. of the tube) made of a steel leaf 0.05 mm thick. The U-shaped ring is stamped from a steel leaf (0.3 mm thick) and has o.d. 22.4 mm, i.d. 11 mm and is 2 mm in height. The void fraction of the carrier (7B) equals to 0.956 m^3/m^3 and specific surface area of 918 m^2/m^3. The detailed information on the experimental methods, investigated carriers and experimentally derived correlations for Fanning friction factor and Nusselt's number can be found in [7]. In general, this structured carrier compared to the classic dumped ceramic ones used so far (half-rings Ø 10 mm × 6 mm × 2 mm and rings Ø 7 mm × 7 mm × 1.5 mm with rounded edges) is characterised by a lower pressure drop (9% vs. 40%) and higher heat transfer coefficients (16% vs. 8%) [7].

3. Catalyst preparation

The selected structured catalyst carrier has been manufactured from steel 00H20J5, containing 20 wt.% of chromium, 5 wt.% of aluminium and traces of carbon. Two methods of support and catalyst layering were used: (1) impregnation in sol solution and (2) Langmuir film deposition which, for the sake of conciseness of this work, is presented in our next paper [10]. The catalyst obtained with the first method was used for kinetic study and for model testing presented in this paper.

The first method of preparation consisted of three steps, which were monitored by X-ray microfluorescence (XRMF)

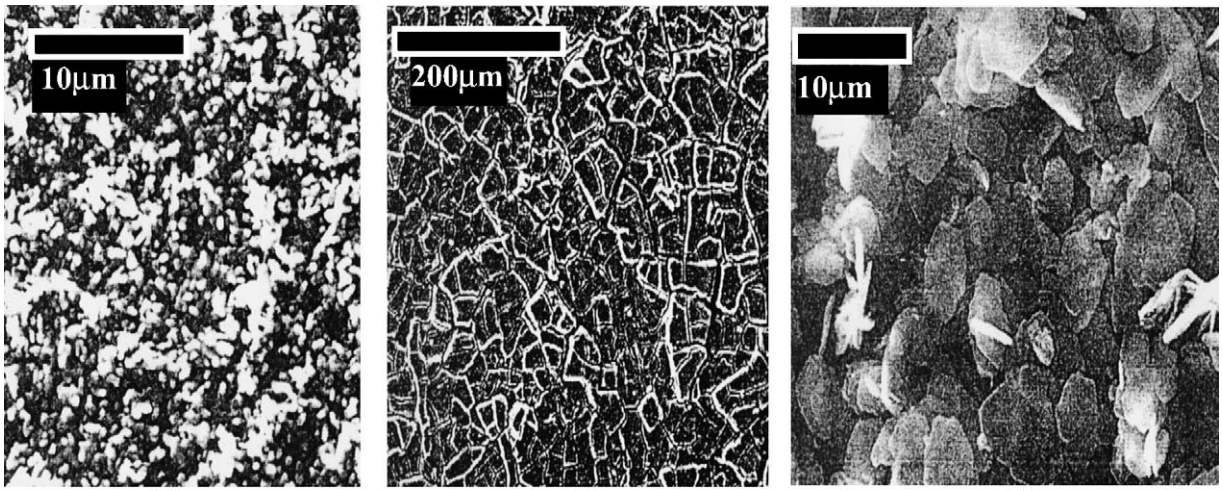

Fig. 1. SEM photographs of the catalyst surface: (A) pre-calcined at 1000 °C (first preparation stage), Al_2O_3 crystallites; (B) wash-coated catalyst surface (second stage), Al–Ti oxide layer; (C) V–P–O precursor deposited (third stage).

and scanning electron microscopy (SEM), Fig. 1A–C. Prior to wash-coat and catalyst depositing the carrier was pre-calcined at 1000 °C for 110 h and then impregnated with Al–Ti sol solution to deposit a wash-coat layer of $Al_2O_3 + TiO_2$. After each impregnation (repeated three times) the carrier was dried at 60 °C to be finally calcined at 500 °C for 2 h. The whole procedure was repeated twice. The catalyst precursor was introduced to the catalyst surface by impregnation with ammonium metavanadate and *o*-phosphoric acid suspended in glycerol (80 wt.% water solution). In order to assure the uniform distribution of the species, the suspension was mixed by bubbling with nitrogen. Impregnation and drying (180 °C, 5 h) was repeated three times. Finally, the catalyst precursor was heated in O_2 to 500 °C at a heating rate 3 °C/min, then calcined for 3 h and cooled at a rate 4 °C/min. The resulting V–P–O catalyst loading amounts approximately 5.3 kg/m^3 of reactor volume and is 11 times lower than that of a classic carrier (dumped ceramic rings Ø5.5 mm × 5.0 mm, 58 kg V–P–O/m^3) used for few comparative reactive tests.

As is seen in SEM photograph (Fig. 1A), on the surface of the calcined steel sheets, firmly attached Al_2O_3 layer is formed. Well-dispersed crystallites of γ-Al_2O_3 in this layer are able to cement the other layers with the carrier body (Fig. 1A). Apparently, during calcination Al atoms diffuse to the surface of steel sheets segregating as a γ-Al_2O_3 phase. The additional $Al_2O_3 + TiO_2$ layer deposited on top of γ–Al_2O_3 creates some sort of a needle-like structure visible in SEM photographs (Fig. 1B). The XRMF analysis shows that the surface is covered mainly with TiO_2 (Ti:Al = 2). The SEM photograph of the final catalyst surface (Fig. 1C) shows in turn a rose-like microstructure similar to that observed by Kamiya et al. [3]. The majority of catalyst surface is covered with a thick uniform layer composed predominantly of V and P, with atomic ratio P:V of about 1, judging from the thorough analysis of both SEM pictures and XRMF surface composition measured exactly at the same zones. There are however, zones covered with a thinner layer of oxides, where P:V ratio is somewhat lower (0.13–0.67) probably due to calcination during which V cations have diffused towards the surface. These zones could display poorer catalytic activity as well as significantly decreased selectivity towards MA as the catalyst composition seems far from the desired structure of vanadyl pyrophosphate $(VO)_2P_2O_7$. The deposition procedure of V–P–O catalyst followed by us has been originally developed for ceramic rings. Thus, taking into account significant differences in shapes and materials of both metallic and ceramic carriers, the catalytic properties appear not optimal (see selectivity of MA formation reported in the next section). For the above reason other methods of catalyst depositing have also been being developed [10].

4. Results of catalytic experiments

The structured catalyst was placed in a laboratory single-tube reactor: i.d. 23.9 mm and 165 mm high. The rosettes and U-rings were stacked alternately. The reactor temperature varying in the range of 360–390 °C was stabilised in a bath of molten salts. The feed of *n*-butane was maintained at a flow rate of 1 dm^3 (STP)/h; air flow rate varied in the range of 30–150 dm^3 (STP)/h. The post-reaction mixtures were analysed by GC–MS supplied with capillary columns (non-polar HP5 and the polar Innowax).

Prior to catalytic experiments, the catalyst was activated under the reaction conditions for 12 h. Initially the catalyst did not show any activity but on conditioning the products appeared, which is frequently reported in the literature, e.g. Kamiya et al. [3]. After 2–3 h the reaction reached a steady-state and the *n*-butane conversion and MA selectivity remained constant.

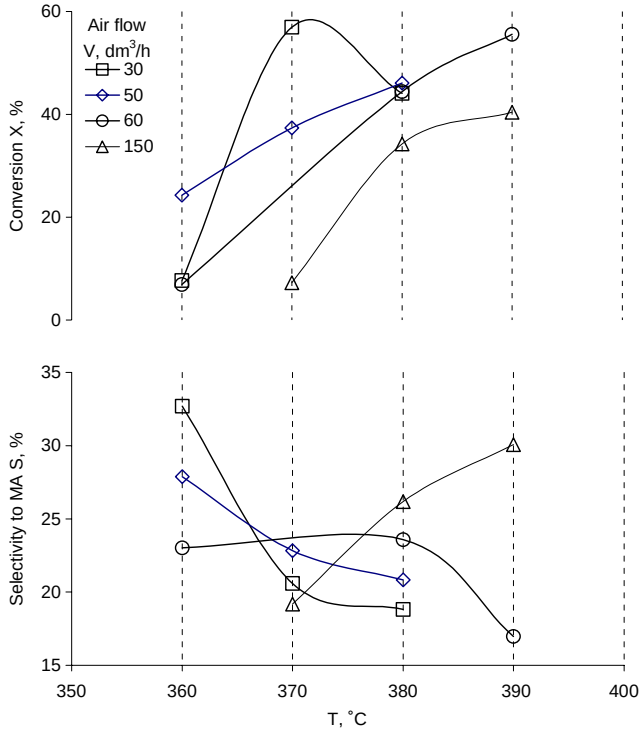

Fig. 2. Temperature dependence on conversion and MA selectivity in *n*-butane oxidation for different air flows (V) dm^3 (STP)/h. *n*-Butane flow was 1 dm^3 (STP)/h for all experiments.

The temperature dependence on the *n*-butane conversion and selectivity towards MA is given in Fig. 2. The reactor operates effectively in a relatively narrow parameter window: over the temperature range of 370–380 °C and at an air flow rate of 50–60 dm^3 (STP)/h. Thus upon increasing the air flow rate to 150 dm^3 (STP)/h and the temperature to 370 °C, *n*-butane conversion decreases markedly. The best catalyst performance was achieved at a air flow rate of 60 dm^3 (STP)/h and a bath temperature of 380 °C.

The results of experiments performed at a flow rate 30 dm^3(STP)/h seem somewhat puzzling, since the conversion having reached the maximum at 370 °C tended to decrease with temperature. Simultaneously, a rapid decrease of MA selectivity was observed at the same flow rate. Such a behaviour could be a result of an experimental error, or even of an unexpected change in the catalyst activity, however equally it could be an inner property of the reacting system.

Two effects could play role here in favouring total oxidation of *n*-butane: the longest contact time and the lowest heat transfer coefficients. The latter result in the highest catalyst temperatures. The reverse temperature dependence on the conversion can be accounted for a huge exothermic effect originating from oxidation of *n*-butane, which contributes to apparent activation energy of the overall reaction (E_{app}) reflected by the values of *n*-butane conversion. This may cause the value of E_{app} to be negative ($E_{app} = E_a + \Delta H$, thus $E_{app} < 0$ if $\Delta H < 0$ and $E_a < |\Delta H|$) giving rise the decrease of conversion with temperature. Moreover, for the considered flow rate, the diffusion coefficients from the bulk gas to the catalyst surface are also the lowest. This may result in *n*-butane deficiency on the catalyst surface, also contributing to the sudden drop of conversion with temperature, and in the increased oxidation in a gaseous phase (decreasing selectivity). However, for better understanding of these complex phenomena more experimental work and modelling should be challenged.

The series of experiments performed at the highest air flow ($V = 150$ dm^3/h, Fig. 2) show a surprising increase of both conversion and selectivity. We decided not to use these data for modelling and evaluation of the reaction rate constants, but to be comprehensive we present them in the Fig. 2. The unusual behaviour could be accounted for by the experimental errors, which may come from diffusional limitation connected with the highest dilution of reactants. Moreover, the inlet section of the reactor might not have reached a proper temperature (inert ballast).

The average conversion observed by us reaches 45% and the average selectivity towards MA: 30%, which seems relatively poor, but what we have to take into account comparing typical conversions obtained in different systems is a reactor space time and a turn-over frequency (catalyst loading). Our test reactor is extremely small (165 mm) in comparison with typical industrial reactors (up to 4 m) and therefore its conversion and selectivity scores cannot be high. Farrauto and Bartholomew [6] report average conversion 80–90% with MA selectivity up to 60% for 4 m long industrial fixed-bed reactors using bulk V–P–O catalyst, while Overbeek [11] for a laboratory reactor—the conversion 5–10% with similar MA selectivity over commercial bulk V–P–O catalyst. Additionally, supported V–P–O catalysts, in contrast to the bulk V–P–O ones, display slightly lower MA selectivity: 30–50% and a higher conversion [11]. The overall *n*-butane conversion on the structured carrier related to the amount of active V–P–O catalyst is almost twice as high as for the dumped ceramic rings (Ø 5.5 mm × 5 mm) with the same catalyst, which were used for comparative tests inside the same reactor and under similar conditions [7]. Furthermore, low MA selectivity observed by us could also be a result of a not efficient or wrong procedure of catalyst preparation on a complicated structure of the metallic carrier.

5. Simplified modelling of reaction kinetics

Diffusive transport of reactants and heat transfer phenomena have been included in a simplified kinetic model. The model assumptions have been derived from experimental results performed within this work (see Fig. 2) and the transport coefficients from the former study [7]. A one-step mechanism of MA formation on catalyst surface has been assumed. The simplified scheme of the parallel reaction is as follows:

$$C_4H_{10} + \nu_1 O_2 \rightarrow MA + (2\nu_1 - 3)H_2O + Q_R \qquad (1a)$$

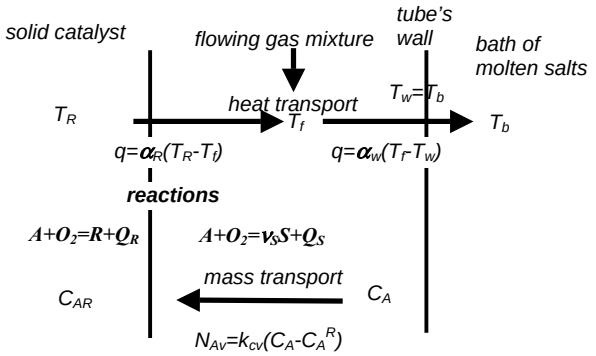

Fig. 3. Scheme of the kinetic model.

$$C_4H_{10} + \nu_2 O_2 \rightarrow \nu_S CO_2 + (2\nu_2 - 2\nu_S)H_2O + Q_S \qquad (1b)$$

In fact *n*-butane is also partly oxidised to CO; the CO:CO_2 ratio 0.8 can be assumed according to Sharma et al. [12]. Thus the heat of total combustion calculated for this contribution of CO and CO_2 amounts to $Q_S = 2158$ kJ/mol: the heat of oxidation towards MA is $Q_R = 1261$ kJ/mol. The stoichiometric factors equal: $\nu_1 = 3.5$; $\nu_2 = 6.5$; $\nu_S = 4$.

The assumptions for the model, envisaged also in Fig. 3, are as follows:

(i) The model of the reaction assumes a simplified heterogeneous mechanism: Diffusion and heat transfer resistances between the fluid and the solid structured catalyst are taken into account. The mass transport is considered as appropriate correction factor, while the heat transfer leads to a more exact estimation of the reaction temperature. Diffusion in the solid catalyst and adsorption are neglected.
(ii) The reactor is unidimensional: The diameter of the reactor was small enough to assume one-dimension reactor model.
(iii) The density of the reacting gas mixture is constant: It has been found that it is approximately constant due to a very high excess of oxygen (from 2 up to 10 times higher than of the stoichiometric values) and to a large amount of diluting gases (nitrogen in air).
(iv) The reaction is of first order with respect to *n*-butane and of zero order—to oxygen: There is an excess of oxygen.
(v) The heat transfer resistance between bath and tube wall is neglected: The heat transfer coefficient from bath to tube (liquid phase—strongly mixed bath of molten salts) is much higher than that from tube to flowing gas.
(vi) Both temperatures of a solid catalyst and flowing gas do not change along the reactor: The length of the reactor is small (165 mm), the energy evolved is relatively low (low conversion degrees and high balance of diluting gases) and the cooling by circulating molten salts is very intensive. Thus, before the reagents reach the catalyst they are thermostated to the temperature of the bath. However, authors are aware of making a rough approximation.
(vii) Reaction towards MA (1a) takes place on catalyst surface, while combustion (1b)–either in a gaseous phase (assumption viiA) or on catalyst surface (assumption viiB).

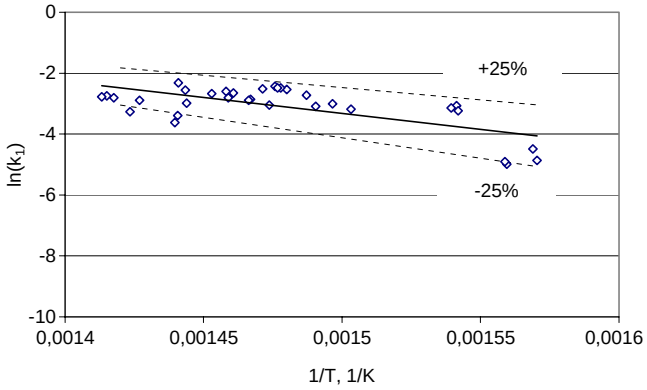

Fig. 4. Arrhenius plot for *n*-butane oxidation to MA derived from a model parameter k_1.

Most of the studies assume catalytic combustion of *n*-butane (1b). However, in our opinion, oxidation of *n*-butane, and especially of CO, may partly take place in a gaseous phase, due to a great excess of oxygen and a relatively high temperature. The problem of homogenous combustion occurring simultaneously with catalytic oxidation is widely discussed for methane selective oxidation. We have also come across similar doubts concerning ammonia oxidation in the literature. Furthermore, the assumption viiA gives lower discrepancies between k_1 values on the Arrhenius plot (Fig. 4) than the assumption viiB. For this reason homogenous combustion is also considered in our calculations. Both assumptions, viiA and viiB, lead to similar equations. The model viiA fits better to the experimental data, however this fact is not an ultimate proof and further works are needed to gain a deeper understanding of a combustion mechanism.

For conciseness, equations derived from different assumptions will be distinguished with a letter "a" or "b" following an equation number. The assumed reaction mechanism gives the following equations:

$$-r_A = -\frac{dC_{Ac}}{d\tau} = k_1 C_{Ac} + k_2 C_A, \qquad r_R = \frac{dC_R}{d\tau} = k_1 C_{Ac},$$

$$r_S = \frac{dC_S}{d\tau} = \nu_S k_2 C_A \qquad (2a)$$

$$r_S = \frac{dC_S}{d\tau} = \nu_S k_2 C_{Ac} \qquad (2b)$$

Mass transfer to the catalyst surface should balance the reaction:

$$k_{cv}(C_A - C_{Ac}) = k_1 C_{Ac} \qquad (3a)$$

$$k_{cv}(C_A - C_{Ac}) = (k_1 + k_2) C_{Ac} \qquad (3b)$$

this gives a diffusional correction:

$$X_D = \frac{k_{cv}}{k_{cv} + k_1}, \qquad k_1^D = k_1 X_D, \qquad C_{Ac} = C_A X_D \tag{4a}$$

$$X_D = \frac{k_{cv}}{k_{cv} + k_1 + k_2}, \qquad k_{1,2}^D = k_{1,2} X_D,$$
$$C_{Ac} = C_A X_D \tag{4b}$$

The conversion degrees are defined as

$$C_{A0}\eta_R = C_R, \qquad C_{A0}\eta_S \nu_S = C_S,$$
$$C_{A0}\eta_A = C_{A0} - C_A, \quad \eta_A = \eta_R + \eta_S \tag{5}$$

Combining Eqs. (2)–(5) the balances of components for an ideal tubular reactor can be then written as

$$d\eta_A = \frac{k_1^D + k_2}{w}(1 - \eta_A)\, dx \tag{6a}$$

$$d\eta_A = \frac{k_1^D + k_2^D}{w}(1 - \eta_A)\, dx \tag{6b}$$

$$d\eta_R = \frac{k_1^D}{w}(1 - \eta_A)\, dx \tag{7}$$

$$d\eta_S = \frac{k_2}{w}(1 - \eta_A)\, dx \tag{8a}$$

$$d\eta_S = \frac{k_2^D}{w}(1 - \eta_A)\, dx \tag{8b}$$

Integration of Eqs. (6)–(8), assuming a constant value of the ratio k_1^D/k_2 (k_1^D/k_2^D) gives

$$-\ln(1 - \eta_A) = k_1^D \left(1 + \frac{\eta_S}{\eta_R}\right) \frac{L}{w} \tag{9}$$

Eq. (9) allows calculating the corrected reaction rate coefficients k_1^D and then true coefficients k_1 (by iteration) for all the catalytic experiments.

To calculate the reaction temperature, energy balance should be considered. According to the assumptions the reaction heat evolved should be balanced by heat transfer to the cooling bath:

$$wC_{A0}(\eta_S Q_S + \eta_R Q_R) = \frac{4L}{D}\alpha_w(T_f - T_w) \tag{10}$$

$$wC_{A0}\eta_R Q_R = La\alpha_c(T_c - T_f) \tag{11a}$$

$$wC_{A0}(\eta_S Q_S + \eta_R Q_R) = La\alpha_c(T_c - T_f) \tag{11b}$$

This leads to the equations for T_c and T_f:

$$T_f = \frac{wC_{A0}D}{4L\alpha_w}(\eta_S Q_S + \eta_R Q_R) + T_w \tag{12}$$

$$T_c = \frac{wC_{A0}\eta_R Q_R}{La\alpha_c} + T_f \tag{13a}$$

$$T_c = \frac{wC_{A0}(\eta_S Q_S + \eta_R Q_R)}{La\alpha_c} + T_f \tag{13b}$$

For the reaction towards MA (2) the Arrhenius equation is

$$k_1 = k_{1,\infty} \exp\left(-\frac{E_1}{RT_c}\right) \tag{14}$$

The Arrhenius plot obtained for assumption viiA is presented in Fig. 4. The value of estimated activation energy is $E_1 = 87$ kJ/mol; and the value of the pre-exponential factor expressed as a boundary rate constant is $k_{1,\infty} = 2.4 \times 10^5$ l/s. Assuming catalytic combustion (assumption viiB), the estimated activation energy was lower ($E_1 = 66$ kJ/mol, $k_{1,\infty} = 10 \times 10^3$ l/s). The values of activation energies obtained by us are comparable to those reported by Sharma et al. [12] for benzene oxidation to MA ($E = 99$ kJ/mol) and by Schneider et al. [13] for *n*-butane oxidation to MA ($E = 72$ kJ/mol). However, the deviation of the calculated k_1 values from the Arrhenius equation is significantly higher for the viiB assumption (correlation factor $R^2 = 0.33$ or scatter of 30%) than for the viiA ($R^2 = 0.46$ or scatter of 25%). First of all, this considerable deviation results from the accuracy of the catalytic experiments. The accuracy of the model simulations is also limited. An average difference between the experiments and calculated conversions amounts to 26% (relative) (for selectivity 16%). The largest deviations exceed 50%. It should be stressed that a series of experiments with the highest air flow rate ($V = 150$ dm^3/h, Fig. 2) are not taken into account during modelling and the estimation of the reaction rate constants because of very high level of experimental errors (possibly a result of high dilution of reactants) and a surprising behaviour of selectivity.

The way of the calculation of the mass transfer coefficients k_{cv} and the heat transfer coefficients α_c and α_w needs some more comments. Mass transfer coefficients k_{cv} as well as heat transfer coefficients α_c between a rosette and flowing gas were calculated using the theoretical solution for mass and heat transfer at a laminar flow. A single segment of the rosette (sector of a circle) has been treated as a representative channel, using its equivalent diameter. Influences of radiation and of free convection have been taken into account. The heat transfer coefficient α_w between the tube wall and the flowing gas was calculated using slightly extrapolated correlation derived by Kolodziej et al. [7].

The model calculations proved that the most significant temperature difference appears between the wall of the reactor and the flowing gas. This difference changes from 7 to 70 K (typically 20–40 K) depending on process conditions. The temperature difference between the gas and the catalyst surface is significantly lower (0.2–0.8 K). This is in a good accordance with calculated differences of *n*-butane concentrations between a gaseous phase (C_A) and the catalyst surface (C_{Ac}). The ratio C_{Ac}:C_A drops in the range of 0.87–0.98 (typically 0.90–0.95). These results are the consequence of a high specific surface area of the structured carrier (over five times higher comparing to that of reactor's tube wall) as well as of an intensive heat and mass transfer inside the short channels formed between the leaves of rosettes. It should be noted that negligence of the heat and

mass transfer resistances between gas and the catalyst significantly influenced estimated values of the activation energy.

6. Conclusions

- Calcination of chromium–aluminium steel—the material for the reactor manufacturing—leads to the formation of a thin layer of γ–Al_2O_3 crystallites strongly connected to the surface.
- The method of depositing TiO_2–Al_2O_3 wash-coat layer has proved efficient for further applications.
- Depositing catalytically active V–P–O phase needs further surveys. The catalyst was not uniformly distributed on the carrier surface due to a complex shape of the rosettes. This could be a reason of a low selectivity towards MA.
- The catalytic tests proved that the structured catalyst could significantly intensify the process of catalytic oxidation. The yield of MA related to the amount of active catalyst was twice as high as that for the classic dumped catalyst.
- A simplified kinetic model has been formulated combining the diffusive transport of reactants as well as the heat transfer phenomena. The value of the activation energy for the formation of MA has been estimated to 87 kJ/mol, which generally agrees with the values reported in other studies.
- The metallic structured carrier with deposited metal oxide catalyst should be profitable for several processes of selective oxidation.

References

[1] M. Malow, Hydrocarb. Process. 59 (1980) 149–153.
[2] G. Centi, F. Cavani, F. Trifiró, Selective Oxidation by Heterogeneous Catalysis, Academic/Plenum Publishers, New York, 2001.
[3] Y. Kamiya, E. Nishikawa, T. Okuhara, T. Hattori, Appl. Catal. A: Gen. 206 (2001) 103–112.
[4] J.R. Ebner, M.R. Thompson, Catal. Today 16 (1993) 15–60.
[5] M.J. Ledoux, C. Crouzet, C. Pham-Huu, V. Turines, K. Koutrakis, P.L. Mills, J.J. Lerou, J. Catal. 203 (2001) 495–508.
[6] R.J. Farrauto C.H. Bartholomew, Fundamentals of Industrial Catalytic Processes, Blackie Academic and Professional, London, 1997.
[7] A. Kolodziej, W. Krajewski, A. Dubis, Catal. Today 69 (2001) 115–120.
[8] W. Krajewski, A. Kolodziej, A. Dubis, Przemysł Chemiczny 82 (2003) 1218–1221 (in Polish).
[9] W. Krajewski, A. Kolodziej, Inserts intensifying heat transfer inside the tubes: design, investigation and performance efficiency criteria, in: Proceedings of the 30th International Conference of Slovak Society of Chemical Engineering, Tatranske Matliare, Slovakia, 2003.
[10] J. Łojewska, A. Kolodziej, P. Dynarowicz, Engineering and chemical aspect of the preparation of microstructural Co_3O_4/Al_2O_3 catalyst for VOC combustion, Catal. Today, submitted for publication.
[11] R.A. Overbeek, New aspects of selective oxidation of *n*-butane to maleic anhydride: the development of a novel catalyst, Ph.D. Thesis, University of Utrecht, Utrecht, 1994.
[12] R.K. Sharma, D.L. Cresswell, E.J. Newson, Selective oxidation of benzene to maleic anhydride at commercially relevant conditions, in: Proceedings of Eighth International Symposium on Chemical Reaction Engineering, I. Chem. E. Symp. Ser. No. 87, 1984, pp. 353–360.
[13] P. Schneider, G. Emig, H. Hoffmann, Ind. Eng. Chem. Res. 26 (1987) 2236–2241.